International Journal of Engineering and Technology Innovation, vol. 7, no. 3, 2017, pp. 188 - 200

The GDQ Method of Thermal Vibration Laminated Shell with Actuating Magnetostrictive Layers

C. C. Hong*

Department of Mechanical Engineering, Hsiuping University of Science and Technology, Taichung, Taiwan, ROC.

Received 01 August 2016; received in revised form 10 January 2017; accepted 11 January 2017

Abstract

The research of laminated magnetostrictive shell under thermal vibration was computed by using the generalized differential quadrature (GDQ) method. In the thermoelastic stress-strain equations that contain the terms linear temperature rise and the magnetostrictive material with velocity feedback control. The dynamic equilibrium differential equations with displacements were normalized and discretized into the dynamic discretized equations by the GDQ method. Two edges of laminated shell with clamped boundary conditions were considered. The values of interlaminar thermal stresses and center displacement of shell with and without velocity feedback control were calculated, respectively. The purpose of this research is to compute the time responses of displacement and stresses in the laminated magnetostrictive shell subjected to thermal vibration with suitable controlled gain values. The numerical GDQ results of displacement and stresses are also obtained and investigated. With velocity feedback and suitable control gain values are found to reduce the amplitude of displacement and stresses into a smaller value. The higher values of temperature get the higher amplitude of displacement and stresses. The GDQ results of actuating magnetostrictive shells can be applied in the field of morphing aircraft (adaptive structures and smart materials) to reduce and suppress the vibration when under aero-thermal flutter.

Keywords: magnetostrictive shell, thermal vibration, GDQ

1. Introduction

Magnetostrictive material can be applied to the fields of sensors and actuators to make the function of faster response. In 2016, Xue et al. [1] designed and modified the injector with magnetostrictive actuator for short responding time of the actuator displacement. Both the numerical and experimental methods were used to compute, measure and validate for the displacement response under the driving voltage. In 2016, Ma et al. [2] used the magnetostrictive metglas composites to establish an active mode non-linear modulation system for magnetoelectric (ME) magnetic sensor. Both the linear and non-linear ME charge coefficient of sensors were calculated and improved. In 2016, Yan et al. [3] applied the magnetostrictive material on the fiber sensor to obtain a rapid and reversible response in wavelength shift. The sensor also had a good future application in the high current field. In 2015, Yang et al. [4] used a feed forward controller in the giant magnetostrictive actuator to simulate a drive servo valve (GMA-DDV). The tracking error in GMA-DDV was greatly decreased with the compound controller. One of the new trends of material in the mechanical engineering is the functionally graded material (FGM). Some special controlled purposes with particular embedded layers are used in the FGM materials, e.g. layers of piezoelectric, magnetostrictive, electrostrictive and shape memory alloys. A commercially available magnetostrictive material Terfenol-D, is in the form of particles embedded easily on the thin layer of main materials without affecting the integrity of structure. And there are some numerical and computational methods used and studied in the fields of composite materials. In 2015, Sadowski et al. [5]

* Corresponding author. E-mail address: cchong@mail.hust.edu.tw

presented the numerical solution for FGM structural elements under mechanical and thermal loads with the finite element (FE) analysis written in the ABAQUS commercial software codes. Both the analytical and numerical methods were used to compute and compare the displacement. In 2013, Sheng and Wang [6] studied the non-linear vibration of cylindrical FGM shells by using analytical method. The possible applications in the future would be in the high-temperature nuclear reactor field. In 2007, Sue et al. [7] presented the numerical results for magnetoelectroelastic bonded antiplane wedge. The singular behavior of the magnetoelectroelastic material was found and in similarly with piezoelectric material. In 2006, Lee et al. [8] provided the non-linear analyses in the laminated composite shells with actuating magnetostrictive layers by using the finite element method (FEM). There were some parametric effects used in the study, e.g. shell type, ratio value of length in axis 1 over radius in axis 2, laminated type, loading and boundary conditions. In 2003, Kumar et al. [9] investigated the FEM computation for the active control of cylindrical shell with magnetostrictive layer. There were two parametric effects used in the study, e.g. clamped-clamped boundary and actuating coils location. Some related inductions of similar experiments research are also included. In 2015, Sharma et al. [10] demonstrated the fuzzy logic controller in the active vibration control for the piezoelectric actuator PZT-5H operating under high temperature to reduce vibration, also found the moderate fluctuations could affect the degraded performance. In 2013, Zhang et al. [11] presented the experimental vibration control tests by using a giant magnetostrictive actuator (GMA) to analyze the non-linear properties for the simplified model, both the properties in low-frequency, micro-level vibration and effectiveness were all improved. In 2008, Olabi and Grunwald [12] presented the advanced applications of magnetostrictive materials for actuators, motors, transducers and sensors, there were a lot of state-of-art designs have been produced in the better properties than conventional materials.

Author also have some investigations in the field of magnetostrictive materials. In 2016, Hong [13] presented the generalized differential quadrature (GDQ) computational results of composite magnetostrictive shells under rapid heating-induced vibration. In 2014, Hong [14] presented the rapid heating vibration analyses of magnetostrictive in circular cylindrical FGM shells by using the GDQ method. In 2013, Hong [15] provided the numerical analyses of thermal vibration in magnetostrictive FGM shells with the GDQ method. It is interesting to study the amplitudes of displacement and interlaminar stresses with and without the effect of velocity feedback, respectively, in the laminated magnetostrictive circular cylindrical shell under thermal vibration by using the GDQ method.

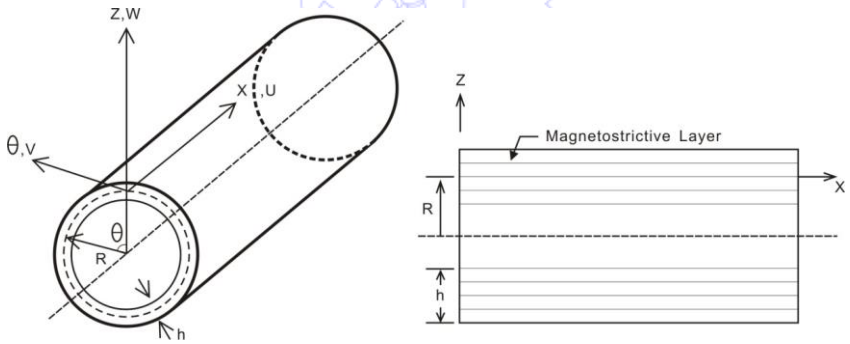

Fig. 1 Geometry of a multilayered shell with magnetostrictive layer

2. Formulation

2.1. Thermoelastic stress-strain relations with magnetostrictive effect

A thin generally orthotropic multilayered circular cylindrical shell is considered as shown in Fig. 1, the stress-strain relationship of the k^{th} layer including thermal strain and magnetostrictive coupling effect can be given in the following equations by Lee et al. [8].

$$\begin{Bmatrix} \sigma_x \\ \sigma_\theta \\ \sigma_{x\theta} \end{Bmatrix}_{(k)} = \begin{bmatrix} \bar{Q}_{11} & \bar{Q}_{12} & \bar{Q}_{16} \\ \bar{Q}_{12} & \bar{Q}_{22} & \bar{Q}_{26} \\ \bar{Q}_{16} & \bar{Q}_{26} & \bar{Q}_{66} \end{bmatrix}_{(k)} \begin{Bmatrix} \varepsilon_x - \alpha_x \Delta T \\ \varepsilon_\theta - \alpha_\theta \Delta T \\ \varepsilon_{x\theta} - \alpha_{x\theta} \Delta T \end{Bmatrix}_{(k)} - \begin{bmatrix} 0 & 0 & \bar{e}_{31} \\ 0 & 0 & \bar{e}_{32} \\ 0 & 0 & \bar{e}_{36} \end{bmatrix}_{(k)} \begin{Bmatrix} 0 \\ 0 \\ \tilde{H}_z \end{Bmatrix} \tag{1}$$

where α_x and α_θ are the coefficients of thermal expansion, $\alpha_{x\theta}$ is the coefficient of thermal shear, ΔT is the temperature difference between the laminate and curing area, $\bar{Q}_{ij}$ is the transformed reduced stiffness, ε_x, ε_θ, $\varepsilon_{x\theta}$ are strains in terms of displacement components, respectively, can be expressed in the following equations.

$$\begin{aligned}\varepsilon_x &= \frac{\partial u}{\partial x} - \frac{\partial^2 w}{\partial x^2} \\ \varepsilon_\theta &= \frac{1}{R}\left(\frac{\partial v}{\partial \theta} + w\right) - \frac{1}{R^2}\left(\frac{\partial^2 w}{\partial \theta^2} - \frac{\partial v}{\partial \theta}\right) z \\ \varepsilon_{x\theta} &= \frac{\partial v}{\partial x} + \frac{1}{R}\frac{\partial u}{\partial \theta} - 2\frac{1}{R}\left(\frac{\partial^2 w}{\partial x \partial \theta} - \frac{\partial v}{\partial x}\right) z\end{aligned} \tag{2}$$

In which u, v and w are displacement components in the x, θ and z direction, respectively. $\bar{e}_{ij}$ is the transformed magnetostrictive coupling module as follows.

$$\begin{aligned}\bar{e}_{31} &= e_{31}\cos^2\theta_* + e_{32}\sin^2\theta_* \\ \bar{e}_{32} &= e_{31}\sin^2\theta_* + e_{32}\cos^2\theta_* \\ \bar{e}_{36} &= (e_{31} - e_{32})\sin\theta_*\cos\theta_*\end{aligned} \tag{3}$$

where θ_* is the angle between fiber direction and axial direction in the laminated layer. R is the mean radius. $\tilde{H}_z$ is the magnetic field intensity, expressed in the following equation. $\tilde{H}_z(x,y,t) = k_c \tilde{I}(x,y,t)$ with velocity feedback control $\tilde{I}(x,y,t) = c(t)\partial w/\partial t$, in which k_c is the coil constant, $\tilde{I}(x,y,t)$ is the coil current, $c(t)$ is the control gain. t is time, thus the value of $k_c c(t)$ would be varied and function of time.

2.2. *Dynamic equilibrium differential equations*

From the Love's theory for thin multilayered shell under the pulsating axial load N_a, the thermally dynamic equilibrium differential equations included the magnetostrictive loads for a stress field in the k^{th} layer can be expressed as follows by Hong et al. [15].

$$\begin{aligned}L_x(u,v,w) &= \rho_t \frac{\partial^2 u}{\partial t^2} \\ L_\theta(u,v,w) + \frac{\partial}{\partial x}\left(N_a \frac{\partial v}{\partial x}\right) &= \rho_t \frac{\partial^2 v}{\partial t^2} \\ L_z(u,v,w) + \frac{\partial}{\partial x}\left(N_a \frac{\partial w}{\partial x}\right) &= \rho_t \frac{\partial^2 w}{\partial t^2}\end{aligned} \tag{4}$$

where t is the time.

$$\begin{aligned}L_x &= \frac{\partial N_x}{\partial x} + \frac{1}{R}\frac{\partial N_{x\theta}}{\partial \theta} \\ L_\theta &= \frac{\partial N_{x\theta}}{\partial x} + \frac{1}{R}\frac{\partial N_\theta}{\partial \theta} + \frac{1}{R}\frac{\partial M_{x\theta}}{\partial x} + \frac{1}{R^2}\frac{\partial M_\theta}{\partial \theta} \\ L_z &= \frac{\partial^2 M_x}{\partial x^2} + \frac{2}{R}\frac{\partial^2 M_{x\theta}}{\partial x \partial \theta} + \frac{1}{R^2}\frac{\partial^2 M_\theta}{\partial \theta^2} - \frac{1}{R}N_\theta \\ \rho_t &= \int_{-h/2}^{h/2} \rho dz\end{aligned}$$

In which ρ is the density, h is the thickness, N_j and M_j are the force and moment resultants, respectively, can be expressed in the following constitutive relations including thermal effect by Lee et al. [8].

$$\begin{bmatrix} N_x \\ N_\theta \\ N_{x\theta} \\ M_x \\ M_\theta \\ M_{x\theta} \end{bmatrix} = \begin{bmatrix} A_{11} & A_{12} & A_{16} & B_{11} & B_{12} & B_{16} \\ A_{12} & A_{22} & A_{26} & B_{12} & B_{22} & B_{26} \\ A_{16} & A_{26} & A_{66} & B_{16} & B_{26} & B_{66} \\ B_{11} & B_{12} & B_{16} & D_{11} & D_{12} & D_{16} \\ B_{12} & B_{22} & B_{26} & D_{12} & D_{22} & D_{26} \\ B_{16} & B_{26} & B_{66} & D_{16} & D_{26} & D_{66} \end{bmatrix} \begin{bmatrix} \partial u/\partial x \\ \frac{1}{R}\left(\frac{\partial v}{\partial \theta} + w\right) \\ \frac{\partial v}{\partial x} + \frac{1}{R}\frac{\partial u}{\partial \theta} \\ -\partial^2 w/\partial x^2 \\ -\frac{1}{R^2}\left(\frac{\partial^2 w}{\partial \theta^2} - \frac{\partial v}{\partial \theta}\right) \\ -\frac{2}{R}\left(\frac{\partial^2 w}{\partial x \partial \theta} - \frac{\partial v}{\partial x}\right) \end{bmatrix} - \begin{bmatrix} \bar{N}_x \\ \bar{N}_\theta \\ \bar{N}_{x\theta} \\ \bar{M}_x \\ \bar{M}_\theta \\ \bar{M}_{x\theta} \end{bmatrix} - \begin{bmatrix} \tilde{N}_x \\ \tilde{N}_\theta \\ \tilde{N}_{x\theta} \\ \tilde{M}_x \\ \tilde{M}_\theta \\ \tilde{M}_{x\theta} \end{bmatrix} \tag{5}$$

where

$$(A_{ij}, B_{ij}, D_{ij}) = \int_{-h/2}^{h/2} \bar{Q}_{ij}\ (1, z, z^2)dz \tag{6}$$

$$(\bar{N}_x, \bar{M}_x) = \int_{-h/2}^{h/2} (\bar{Q}_{11}\alpha_x + \bar{Q}_{12}\alpha_\theta + \bar{Q}_{16}\alpha_{x\theta})\Delta T(1, z)dz$$

$$(\bar{N}_\theta, \bar{M}_\theta) = \int_{-h/2}^{h/2} (\bar{Q}_{12}\alpha_x + \bar{Q}_{22}\alpha_\theta + \bar{Q}_{26}\alpha_{x\theta})\Delta T(1, z)dz \tag{7}$$

$$(\bar{N}_{x\theta}, \bar{M}_{x\theta}) = \int_{-h/2}^{h/2} (\bar{Q}_{16}\alpha_x + \bar{Q}_{26}\alpha_\theta + \bar{Q}_{66}\alpha_{x\theta})\Delta T(1, z)dz$$

$$\begin{bmatrix} \tilde{N}_x \\ \tilde{N}_\theta \\ \tilde{N}_{x\theta} \end{bmatrix} = \sum_{k=1}^{N_m} \int_{z_k}^{z_{k+1}} \begin{bmatrix} \bar{e}_{31} \\ \bar{e}_{32} \\ \bar{e}_{36} \end{bmatrix}^{(k)} \tilde{H}_z dz \tag{8}$$

$$\begin{bmatrix} \tilde{M}_x \\ \tilde{M}_\theta \\ \tilde{M}_{x\theta} \end{bmatrix} = \sum_{k=1}^{N_m} \int_{z_k}^{z_{k+1}} \begin{bmatrix} \bar{e}_{31} \\ \bar{e}_{32} \\ \bar{e}_{36} \end{bmatrix}^{(k)} \tilde{H}_z z^2 dz \tag{9}$$

where the N_m represents the number of layer of magnetostrictive material.

Firstly, the behaviors of a multi-layered shell constructed of orthotropic layers are considered, the following terms A_{16}, A_{26}, D_{16}, D_{26} are all zero. Substituting the Eq. (5) into Eq. (4), the equilibrium differential equations in terms of displacement components u, v and w can be obtained and shown in Appendix 1.

2.3. *Dynamic discretized equations*

The vibration case is considered for the condition of expansion strain distribution which is independent of x and θ and an even function of z ($\bar{M}_x = \bar{M}_\theta = \bar{M}_{x\theta} = 0$), using $\bar{N}_x$ =-N_a x, $\Delta T = T_0 x A_{11}/R^2$ as the thermally initial expansion load which is dependent of x, T_0 is thermal load temperature and treating the following displacement components.

$$\begin{aligned} u &= U(x)\cos(n\theta + \omega t) \\ v &= V(x)\sin(n\theta + \omega t) \\ w &= W(x)\cos(n\theta + \omega t) \end{aligned} \tag{10}$$

where ω (rad/sec) is the natural circular frequency and n is an integer for the circumferential wave number of the multi-layered shell. Thus, the values of displacement components u, v and w would be varied and function of time.

The GDQ method was presented by Shu and Richards and can be restated that: the derivative of a smooth function at a discrete point in a domain can be discretized by using an approximated weighting linear sum of the function values at all the discrete points in the direction by Shu and Du in 1997 [16], Bert et al. in 1989 [17]. One-dimensional GDQ method is applied to discretize the equilibrium differential equation, the following non-dimensional parameters are introduced.

$$X = x/L,\ U = U(x)/L,\ V = V(x)/R\ W = W(x)/h,\ Z = Z/h$$

where L is the length of shell.

The discretized equilibrium equation at the i^{th} discrete point $X = X_i$ can be obtained. For two edges are clamped, symmetric ($B_{ij} = 0$), orthotropic ($A_{16} = A_{26} = 0$, $D_{16} = D_{26} = 0$, $\alpha_{x\theta} = 0$) of laminated shell under temperature loading, the following boundary condition is applicable.

At x = 0 and L:

$$u = v = w = \partial w/\partial x = 0 \tag{11}$$

After the process of non-dimension and discretization for the boundary condition (11), the following equation is given.

At X = 0 and 1:

$$U_1 = U_N = V_1 = V_N = W_1 = W_N = \sum_{l=1}^{N} A_{1,l}^{(1)} W_l = \sum_{l=1}^{N} A_{N,l}^{(1)} W_l = 0 \tag{12}$$

Now considering and implementing the given eight boundary conditions (12) at both clamped ends of the multilayered shell on the discretized equilibrium equation for the all interior grid points i=2,3,...,N-1, then the normalized and discretized equations can be obtained and shown in Appendix 2. And the frequency parameter is defined as $f^* = \omega R\sqrt{\rho_t / A_{11}}$. When the displacements have been solved, then the thermal stresses in discretized equation of the k^{th} layer can be found and shown in Appendix 3.

3. Computational Results

The following coordinate for the grid point is used in the GDQ computation.

$$x_i = 0.5[1-\cos(\frac{i-1}{N-1}\pi)]L,\ i = 1,2,...,N \tag{13}$$

The total three-layer ($0^{om}/90^{o}/0^{o}$) cross-ply laminated shell with the upper surface magnetostrictive layer, the inner layer and outer layer of typical host materials are considered. The superscript of m denotes magnetostrictive material. Each layer has the same thickness. The material properties of the typical inner, outer of host material, magnetostrictive material are listed in the Table 1. The magnetostrictive Terfenol-D coupling module is $e_{31}=e_{32}=E^m d^m$ and E^m=26.5 GPa, d^m=1.67*10^{-8} mA^{-1}.

Table 1 Properties of typical host and Terfenol-D

Properties	Typical host		Terfenol-D
	Inner	Outer	
$\frac{E_1}{E_2}$	25	40	1
$\frac{G_{12}}{E_2}$	0.5	0.6	$\frac{13.25}{26.5}$
ν_{12}	0.15	0.27	0.0
$\rho(lb/in^3)$	0.087	0.283	0.334179
$\alpha_x(1/°F)$	6×10^{-6}	6.5×10^{-6}	12×10^{-6}
$\alpha_\theta(1/°F)$	6×10^{-6}	6.5×10^{-6}	12×10^{-6}

Table 2 GDQ convergence for ($0^{om}/90^{o}/0^{o}$)

N	f^*	$W(L/2)$
23	0.0128564	0.944165
41	0.0128571	0.913904
49	0.0128564	0.914536
73	0.0128564	0.915959

Firstly, to investigate the dynamic convergence of the frequency parameter f^* and center displacement $W(L/2)$ with R/h=500, L/R=10, circumferential wave number n=4, T_0=100°F, θ=1 radian, time t=1 sec and $k_c c(t)$=0 under clamped-clamped boundary condition. Table 2 shows the f^* and $W(L/2)$ with respect to N for ($0^{om}/90^{o}/0^{o}$) laminated magnetostrictive shell. The data accuracies of f^* and $W(L/2)$ are 0.0 and 0.001553, respectively. The N=73 grid point has the good convergence results are found and can be used further in the GDQ computation of time responses for deflection and stress with suitable $k_c c(t)$ values to reduce the amplitude of displacement.

The calculating data in this research have been contrasted with the reference test data. Table 3 re-listed the frequency parameter f^* with controlled values $k_c c(t)$=0 for three-layer ($0^{om}/90^{o}/0^{o}$), ($0^{o}/90^{om}/0^{o}$) and ($0^{o}/90^{o}/0^{om}$) of thin laminated magnetostrictive shells by using the GDQ method, compared with the available data of papers from Hong [13] in 2016. They are considered in acceptable values.

Table 3 Comparison of f^*

Thin isotropic tube	GDQ computational solution in 2015		Dym's exact solution in 1973	Chung's series solution in 1981	
	N	f^*	f^*	Terms	f^*
	18	0.0150848	0.01508	500	0.01508
Thin laminated magnetostrictive shell	GDQ solution, N=73, superscript of m: Terfenol-D				
	$(0^{om}/90^{o}/0^{o})$		$(0^{o}/90^{om}/0^{o})$	$(0^{o}/90^{o}/0^{om})$	
	f^*		f^*	f^*	
	0.0128564		0.0210714	0.0135714	

Fig. 2 shows the dominant normal displacement W along X under $\Delta T=T_0 x A_{11}/R^2$, T_0=100° F, θ=1 radian, time t =1 sec, N=73, for $(0^{om}/90^{o}/0^{o})$ laminated magnetostrictive shell by using the GDQ method. The amplitude of displacement W is large when without velocity feedback $k_c c(t)$=0. With velocity feedback and with suitable values $k_c c(t)=10^6$ are found and can reduce the amplitude of displacement to a smaller value. (from 0.928012 at $k_c c(t)$=0 to 0.045060 at $k_c c(t)=10^6$). By using the higher gain value e.g. $k_c c(t)=10^6$, the amplitude reducing ratio of W can be around to 21 for $(0^{om}/90^{o}/0^{o})$.

Fig. 3 shows the dominant thermal stress $\bar{\sigma}_\theta=\sigma_\theta/E_2$ on Z=-1/6 along X under $\Delta T=T_0 x A_{11}/R^2$, T_0=100° F, θ=1 radian, time t=1sec, N=73, for $(0^{om}/90^{o}/0^{o})$ laminated magnetostrictive shell by using the GDQ method. The amplitude of thermal stress $\bar{\sigma}_\theta$ is large when without velocity feedback $k_c c(t)$=0. With velocity feedback and with suitable values $k_c c(t)=10^6$ are found and can also reduce the amplitude of thermal stress $\bar{\sigma}_\theta$ to a smaller value. (from 0.007680 at k_c $c(t)$= 0 to 0.000552 at $k_c c(t)=10^6$ and the curves decline clockwise an angle with X=0 axis). By using the higher gain value e.g. $k_c c(t)=10^6$, the amplitude reducing ratio of $\bar{\sigma}_\theta$ can be around to 14 for $(0^{om}/90^{o}/0^{o})$.

Fig. 4 shows the dominant normal displacement W along X under $\Delta T=T_0 x A_{11}/R^2$, T_0=100° F, θ=1 radian, time t=1 sec, N=73, for $(0^{om}/0^{o}/0^{o})$ laminated magnetostrictive shell by using the GDQ method. The amplitude of displacement W is large when without velocity feedback $k_c c(t)$=0. With velocity feedback and with suitable values $k_c c(t)=10^6$ are found and can reduce the amplitude of displacement to a smaller value. (from 0.776466 at $k_c c(t)$=0 to 0.049256 at $k_c c(t)=10^6$). By using the higher gain value e.g. $k_c c(t)=10^6$, the amplitude reducing ratio of W can be around to 16 for $(0^{om}/0^{o}/0^{o})$.

Fig. 5 shows the dominant thermal stress $\bar{\sigma}_x=\sigma_x/E_2$ on Z=-1/6 along X under $\Delta T=T_0 x A_{11}/R^2$, T_0=100° F, θ=1 radian, time t=1sec, N=73, for $(0^{om}/0^{o}/0^{o})$ laminated magnetostrictive shell by using the GDQ method. Without velocity feedback and with suitable values $k_c c(t)=10^6$ are found and almost have the same amplitude of thermal stress $\bar{\sigma}_x$ at time t=1sec (0.000359 and the curves decline clockwise an angle with X=0 axis). The values of control gain do not affect the amplitude reducing ratio of $\bar{\sigma}_x$ for $(0^{om}/0^{o}/0^{o})$.

Fig. 6 shows the dominant normal displacement W along X under $\Delta T=T_0 x A_{11}/R^2$, with respect to T_0= T_0=0° F, 250° F, 500° F, respectively, without velocity feedback $k_c c(t)$=0, θ=1 radian, time t=1sec, N=73, for $(0^{om}/90^{o}/0^{o})$ laminated magnetostrictive shell by using the GDQ method. The amplitude of displacement W is larger when T_0=500° F. The higher values of temperature get the higher amplitude of displacement are found (from 4.658570 at T_0=500° F to 2.331650 at T_0=250° F). Under the higher temperature value e.g. T_0=500° F and 250° F, the amplitude raising ratio of W can be around to 2 for $(0^{om}/90^{o}/0^{o})$.

Fig. 7 shows the dominant thermal stress $\bar{\sigma}_\theta$ on Z=-1/6 along X under $\Delta T=T_0 x A_{11}/R^2$, with respect to T_0=0° F, 250° F, 500° F, respectively, without velocity feedback $k_c c(t)$=0, θ=1 radian, time t=1sec, N=73, for $(0^{om}/90^{o}/0^{o})$ laminated magnetostrictive shell by using the GDQ method. The amplitude of thermal stress $\bar{\sigma}_\theta$ is larger when T_0=500° F. The higher

values of temperature get the higher amplitude of thermal stress $\bar{\sigma}_\theta$ are found (from 0.0386192 at T_0=500$^\circ F$ to 0.0193308 at T_0=250$^\circ F$). Under the higher temperature value e.g. T_0=500$^\circ F$ and 250$^\circ F$, the amplitude raising ratio of $\bar{\sigma}_\theta$ can be around to 2 for ($0^{\circ m}$/90°/0°).

Fig. 8 shows the dominant normal displacement W along X under $\Delta T = T_0 x A_{11}/R^2$, with respect to T_0=0$^\circ F$, 250$^\circ F$, 500$^\circ F$, respectively, without velocity feedback $k_c c(t)$=0, θ=1 radian, time t=1sec, N=73, for ($0^{\circ m}$/90°/0°) laminated magnetostrictive shell by using the GDQ method. The amplitude of displacement W is larger when T_0=500$^\circ F$. The higher values of temperature get the higher amplitude of displacement are found (from 3.739460 at T_0=500$^\circ F$ to 1.868050 at T_0=250$^\circ F$). Under the higher temperature value e.g. T_0=500° F and 250° F, the amplitude raising ratio of W can be around to 2 for ($0^{\circ m}$/90°/0°).

Fig. 9 shows the dominant thermal stress $\bar{\sigma}_x$ on Z=-1/6 along X under $\Delta T = T_0 x A_{11}/R^2$, with respect to T_0=0$^\circ F$, 250$^\circ F$, 500° F, respectively, without velocity feedback $k_c c(t)$=0, θ=1 radian, time t=1sec, N=73, for ($0^{\circ m}$/90°/0°) laminated magnetostrictive shell by using the GDQ method. The amplitude of thermal stress $\bar{\sigma}_x$ is larger when T_0=500$^\circ F$. The higher values of temperature get the higher values, linearly of thermal stress $\bar{\sigma}_x$ are found (from 0.065532 at T_0=500$^\circ F$ to 0.0327377 at T_0=250$^\circ F$). Under the higher temperature value e.g. T_0=500$^\circ F$ and 250$^\circ F$, the amplitude raising ratio of $\bar{\sigma}_x$ can be around to 2 for ($0^{\circ m}$/90°/0°).

Fig. 10 shows the time response of dominant normal displacement W at X=0.543578 with respect to time t =1, 100, 200, 300, 400, and 500 sec, respectively, under $\Delta T = T_0 x A_{11}/R^2$, T_0=100$^\circ F$, θ=1 radian, N=73, without velocity feedback $k_c c(t)$=0 and with suitable values $k_c c(t)$=10^6, for ($0^{\circ m}$/90°/0°) laminated magnetostrictive shell by using the GDQ method. With velocity feedback and with suitable values $k_c c(t)$=10^6 are found and can reduce the amplitude of displacement to a smaller value (from 0.928012 at $k_c c(t)$=0 to 0.045060 at $k_c c(t)$=10^6). By using the higher gain value e.g. $k_c c(t)$=10^6, the amplitude reducing ratio of W can be around to 21 for ($0^{\circ m}$/90°/0°).

Fig. 11 shows the time response of dominant thermal stress $\bar{\sigma}_\theta$ at X=0.543578, Z=-1/6 with respect to time t =1, 100, 200, 300, 400, and 500 sec, respectively, under $\Delta T = T_0 x A_{11}/R^2$, T_0=100° F, θ=1 radian, N=73, without velocity feedback $k_c c(t)$=0 and with suitable values $k_c c(t)$=10^6, for ($0^{\circ m}$/90°/0°) laminated magnetostrictive shell by using the GDQ method. With velocity feedback and with suitable values $k_c c(t)$=10^6 are found and can reduce the amplitude of thermal stress $\bar{\sigma}_\theta$ to a smaller value (from 0.101244 at $k_c c(t)$=0 to 0.002496 at $k_c c(t)$=10^6). By using the higher gain value e.g. $k_c c(t)$=10^6, the amplitude reducing ratio of $\bar{\sigma}_\theta$ can be around to 40 for ($0^{\circ m}$/90°/0°).

Fig. 12 shows the time response of dominant normal displacement W at X=0.768650, with respect to time t =1, 100, 200, 300, 400, and 500 sec, respectively, under $\Delta T = T_0 x A_{11}/R^2$, T_0=100$^\circ F$, θ=1 radian, N=73, without velocity feedback $k_c c(t)$=0 and with suitable values $k_c c(t)$=10^6, for ($0^{\circ m}$/90°/0°) laminated magnetostrictive shell by using the GDQ method. With velocity feedback and with suitable values $k_c c(t)$=10^6 are found and can reduce the amplitude of displacement to a smaller value (from 0.776466 at $k_c c(t)$=0 to 0.169729 at $k_c c(t)$=10^6). By using the higher gain value e.g. $k_c c(t)$=10^6, the amplitude reducing ratio of W can be around to 5 for ($0^{\circ m}$/90°/0°).

Fig. 13 shows the time response of dominant thermal stress $\bar{\sigma}_x$ at X=0.768650, Z=-1/6 with respect to time t =1, 100, 200, 300, 400, and 500 sec, respectively, under $\Delta T = T_0 x A_{11}/R^2$, T_0=100° F, θ=1 radian, N=73, without velocity feedback $k_c c(t)$=0 and with suitable values $k_c c(t)$=10^6, for ($0^{\circ m}$/90°/0°) laminated magnetostrictive shell by using the GDQ method. With velocity feedback and with suitable values $k_c c(t)$=10^6 are found and can reduce the amplitude of thermal stress $\bar{\sigma}_x$ to a

smaller value (from 0.001245 at $k_c c(t)=0$ to 0.000765 at $k_c c(t)=10^6$). By using the higher gain value e.g. $k_c c(t)=10^6$, the amplitude reducing ratio of $\bar{\sigma}_x$ can be around to 2 for ($0^{om}/90^{o}/0^{o}$).

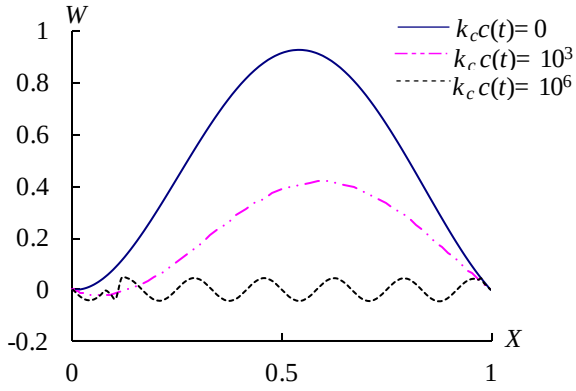

Fig. 2 W along X for ($0^{om}/90^{o}/0^{o}$)

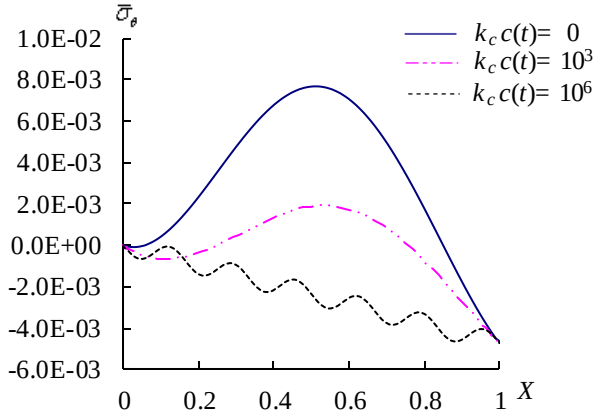

Fig. 3 $\bar{\sigma}_\theta$ along X for ($0^{om}/90^{o}/0^{o}$)

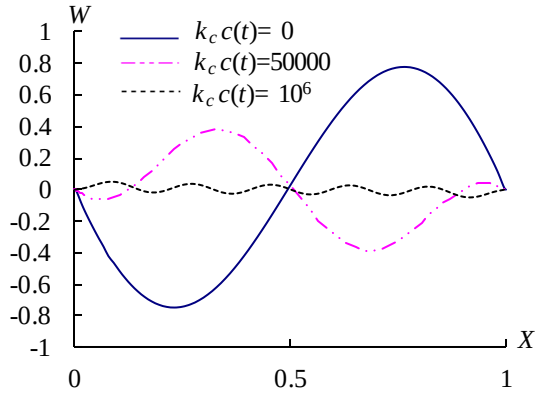

Fig. 4 W along X for ($0^{om}/90^{o}/0^{o}$)

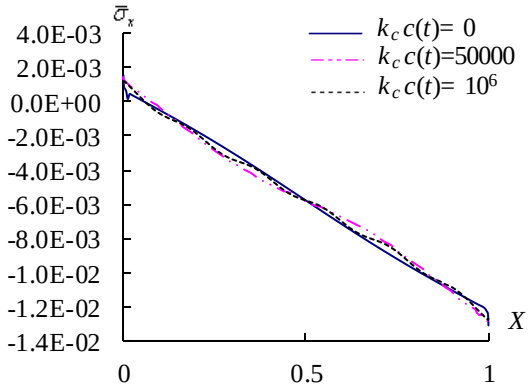

Fig. 5 $\bar{\sigma}_x$ along X for ($0^{om}/90^{o}/0^{o}$)

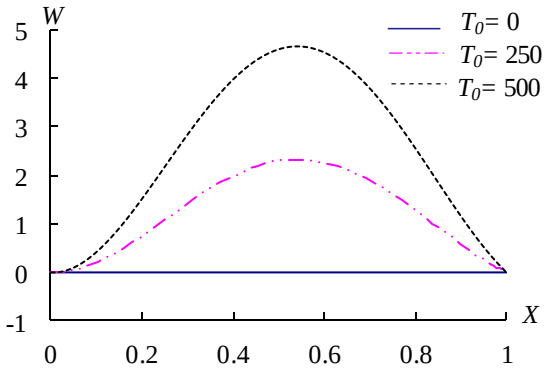

Fig. 6 W along X for ($0^{om}/90^{o}/0^{o}$)

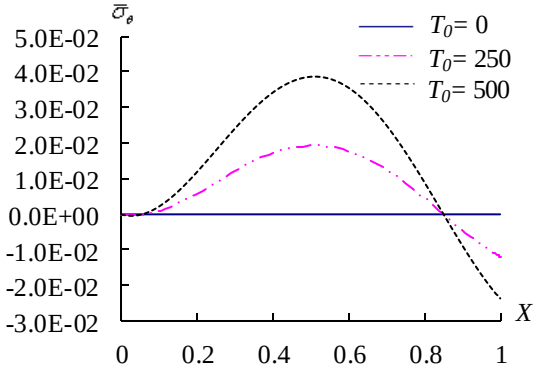

Fig. 7 $\bar{\sigma}_\theta$ along X for ($0^{om}/90^{o}/0^{o}$)

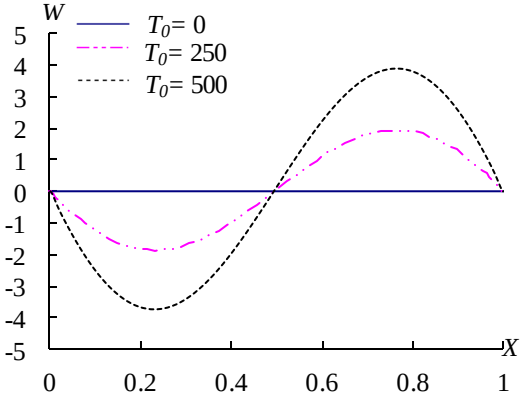

Fig. 8 W along X for ($0^{om}/90^{o}/0^{o}$)

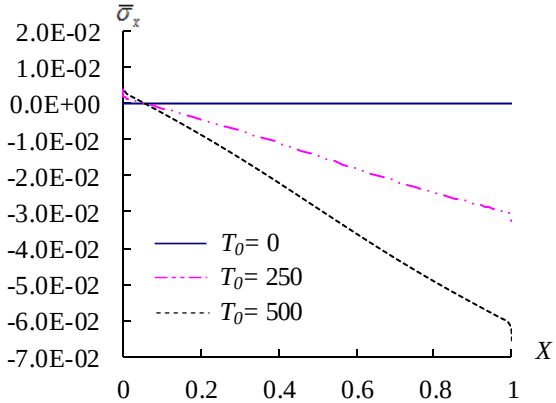

Fig. 9 $\bar{\sigma}_x$ along X for ($0^{om}/90^{o}/0^{o}$)

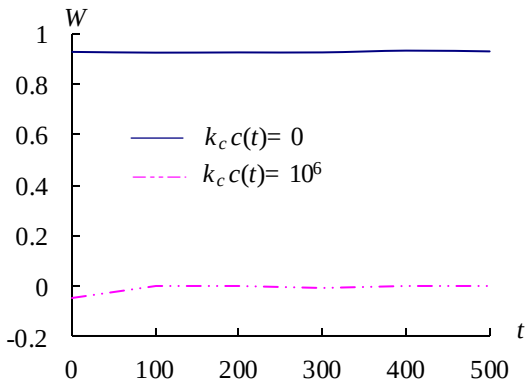

Fig. 10 W vs. t for (0^{om}/90^{o}/0^{o})

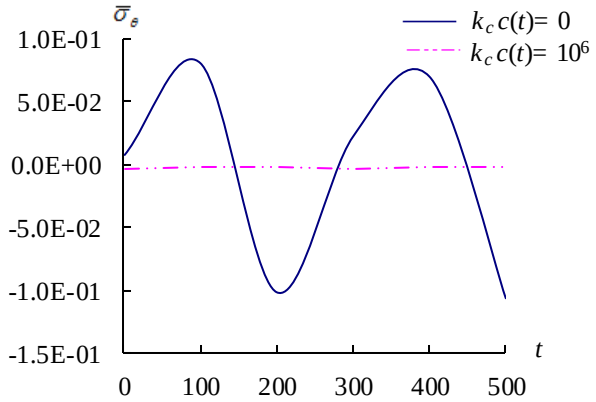

Fig. 11 $\bar{\sigma}_\theta$ vs. t for (0^{om}/90^{o}/0^{o})

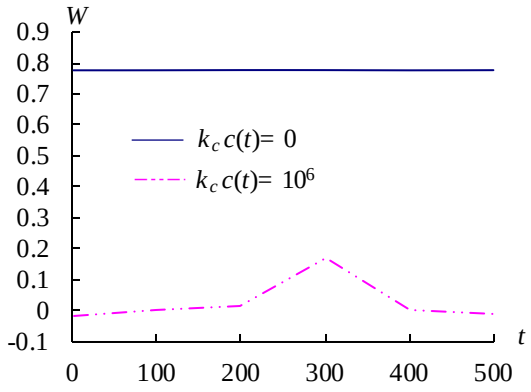

Fig. 12 W vs. t for (0^{om}/90^{o}/0^{o})

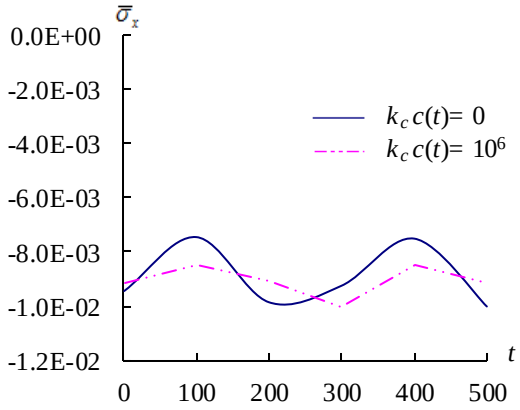

Fig. 13 $\bar{\sigma}_x$ vs. t for (0^{om}/90^{o}/0^{o})

4. Conclusions

The GDQ method can be successfully applied to compute the time responses of displacement and stresses in the laminated magnetostrictive shell subjected to thermal vibration. With velocity feedback and with suitable values of $k_c c(t)$ are found and can reduce the amplitude of displacement and stresses to a smaller value. The higher values of temperature get the higher amplitude of displacement and stresses.

References

[1] G. Xue, P. Zhang, Z. He, D. Li, Z. Yang and Z. Zhao, "Displacement model and driving voltage optimization for a giant magnetostrictive actuator used on a high-pressure common-rail injector," Materials and Design, vol. 95, no. 5, pp. 501-509, 2016.

[2] J. Ma, J. Jiao, C. Fang, X. Zhao and H. Luo, "High sensitive nonlinear modulation magnetoelectric magnetic sensors with a magnetostrictive metglas structure based on bell-shaped geometry," Journal of Magnetism and Magnetic Materials, vol. 405, no. 1, pp. 225-230, 2016.

[3] H. Yan, X. Zhao, C. Zhang, Z. Zhen, Z. Zhang, L. Li and D. Han, "A novel current fiber sensor with magnetostrictive material based on the plasmon response," Optik - International Journal for Light and Electron Optics, vol. 127, no. 3, pp. 1323-1325, 2016.

[4] Z. Yang, Z. He, D. Li, J. Yu, X. Cui and Z. Zhao, "Direct drive servo valve based on magnetostrictive actuator: multi-coupled modeling and its compound control strategy," Sensors and Actuators A: Physical, vol. 235, pp. 119-130, 2015.

[5] T. Sadowski, M. Bîrsan and D. Pietras, "Multilayered and FGM structural elements under mechanical and thermal loads. Part I: Comparison of finite elements and analytical models," Archives of Civil and Mechanical Engineering, vol. 15, no. 4, pp. 1180-1192, 2015.

[6] G. G. Sheng and X. Wang "An analytical study of the non-linear vibrations of functionally graded cylindrical shells subjected to thermal and axial loads," Composite Structures, vol. 97, pp. 261-268, 2013.

[7] W. C. Sue, J. Y. Liou and J. C. Sung, "Investigation of the stress singularity of a magnetoelectroelastic bonded antiplane wedge," Applied Mathematical Modelling, vol. 31, no. 10, pp. 2313-2331, 2007.
[8] S. J. Lee, J. N. Reddy and F. Rostam-Abadi, "Nonlinear finite element analysis of laminated composite shells with actuating layers," Finite Elements in Analysis and Design, vol. 43, no. 1, pp. 1-21, 2006.
[9] J. S. Kumar, N. Ganesan, S. Swarnamani and C. Padmanabhan, "Active control of cylindrical shell with magnetostrictive layer," Journal of Sound and Vibration, vol. 262, no. 3, pp. 577-589, 2003.
[10] A. Sharma, R. Kumar, R. Vaish, V. S. Chauhan, "Active vibration control of space antenna reflector over wide temperature range," Composite Structures, vol. 128, pp. 291-304, 2015.
[11] T. Zhang, B. T. Yang, H. G. Li, G. Meng, "Dynamic modeling and adaptive vibration control study for giant magnetostrictive actuators," Sensors and Actuators A: Physical, vol. 190, pp. 96-105, 2013.
[12] A. G. Olabi, A. Grunwald, "Design and application of magnetostrictive materials," Materials & Design, vol. 29, no. 2, pp. 469-483, 2008.
[13] C. C. Hong, "Rapid heating-induced vibration of composite magnetostrictive shells," Mechanics of Advanced Materials and Structures, vol. 23, no. 4, pp. 415-422, 2016.
[14] C. C. Hong, "Rapid heating induced vibration of circular cylindrical shells with magnetostrictive functionally graded material," Archives of Civil and Mechanical Engineering, vol. 14, no. 4, pp. 710-720, 2014.
[15] C. C. Hong, "Thermal vibration of magnetostrictive functionally graded material shells," European Journal of Mechanics-A/Solids, vol. 40, pp. 114-122, 2013.
[16] C. Shu and H. Du, "Implementation of clamped and simply supported boundary conditions in the GDQ free vibration analyses of beams and plates," International Journal of Solids and Structures, vol. 34, no. 7, pp. 819-835, 1997.
[17] C. W. Bert, S. K. Jang and A. G. Striz, "Nonlinear bending analysis of orthotropic rectangular plates by the method of differential quadrature," Computational Mechanics, vol. 5, no. 2, pp. 217-226, 1989.

Appendix 1.

The equilibrium differential equations in terms of displacement components u, v and w are shown as follows.

$$\begin{bmatrix} L_{11} & L_{12} & L_{13} \\ L_{21} & L_{22} & L_{23} \\ L_{31} & L_{32} & L_{33} \end{bmatrix} \begin{bmatrix} u \\ v \\ w \end{bmatrix} = \begin{bmatrix} b_1 \\ b_2 \\ b_3 \end{bmatrix} \tag{A1}$$

where

$$L_{11} = A_{11}\frac{\partial^2}{\partial x^2} + \frac{A_{66}}{R^2}\frac{\partial^2}{\partial \theta^2} - \rho_t \frac{\partial^2}{\partial t^2}$$

$$L_{12} = (\frac{B_{12}}{R^2} + \frac{A_{12}}{R} + \frac{A_{66}}{R} + 2\frac{B_{66}}{R^2})\frac{\partial^2}{\partial x \partial \theta}$$

$$L_{13} = \frac{A_{12}}{R}\frac{\partial}{\partial x} - B_{11}\frac{\partial^3}{\partial x^3} - (\frac{B_{12}}{R^2} + 2\frac{B_{66}}{R^2})\frac{\partial^3}{\partial x \partial \theta^2}$$

$$L_{21} = (\frac{B_{12}}{R^2} + \frac{A_{12}}{R} + \frac{A_{66}}{R} + \frac{B_{66}}{R^2})\frac{\partial^2}{\partial x \partial \theta}$$

$$L_{22} = (A_{66} + \frac{3B_{66}}{R} + \frac{2D_{66}}{R^2})\frac{\partial^2}{\partial x^2} + (\frac{2B_{22}}{R^3} + \frac{A_{22}}{R^2} + \frac{D_{22}}{R^4})\frac{\partial^2}{\partial \theta^2} - \rho_t \frac{\partial^2}{\partial t^2} + \frac{\partial}{\partial x}(N_a \frac{\partial}{\partial x})$$

$$L_{23} = (\frac{A_{22}}{R^2} + \frac{B_{22}}{R^3})\frac{\partial}{\partial \theta} - (\frac{2B_{66}}{R} + \frac{B_{12}}{R} + \frac{2D_{66}}{R^2} + \frac{D_{12}}{R^2})\frac{\partial^3}{\partial x^2 \partial \theta} - (\frac{B_{22}}{R^3} + \frac{D_{22}}{R^4})\frac{\partial^3}{\partial \theta^3}$$

$$L_{31} = -\frac{A_{12}}{R}\frac{\partial}{\partial x} + B_{11}\frac{\partial^3}{\partial x^3} + (\frac{B_{12}}{R^2} + 2\frac{B_{66}}{R^2})\frac{\partial^3}{\partial x \partial \theta^2}$$

$$L_{32} = -(\frac{A_{22}}{R^2} + \frac{B_{22}}{R^3})\frac{\partial}{\partial \theta} + (\frac{2B_{66}}{R} + \frac{B_{12}}{R} + \frac{4D_{66}}{R^2} + \frac{D_{12}}{R^2})\frac{\partial^3}{\partial x^2 \partial \theta} + (\frac{B_{22}}{R^3} + \frac{D_{22}}{R^4})\frac{\partial^3}{\partial \theta^3}$$

$$L_{33} = \frac{2B_{12}}{R} - D_{11}\frac{\partial^4}{\partial x^4} - (\frac{2D_{12}}{R^2} + \frac{4D_{66}}{R^2})\frac{\partial^4}{\partial x^2 \partial \theta^2} - \frac{D_{22}}{R^4}\frac{\partial^4}{\partial \theta^4} + \frac{2B_{22}}{R^3}\frac{\partial^2}{\partial \theta^2} - \frac{A_{22}}{R^2} - \rho_t \frac{\partial^2}{\partial t^2} + \frac{\partial}{\partial x}(N_a \frac{\partial}{\partial x})$$

$$b_1 = \frac{\partial \overline{N}_x}{\partial x} + \frac{1}{R}\frac{\partial \overline{N}_{x\theta}}{\partial \theta} + \frac{\partial \widetilde{N}_x}{\partial x} + \frac{1}{R}\frac{\partial \widetilde{N}_{x\theta}}{\partial \theta}$$

$$b_2 = \frac{\partial \overline{N}_{x\theta}}{\partial x} + \frac{1}{R}\frac{\partial \overline{N}_\theta}{\partial \theta} + \frac{1}{R}\frac{\partial \overline{M}_{x\theta}}{\partial x} + \frac{1}{R^2}\frac{\partial \overline{M}_\theta}{\partial \theta} + \frac{\partial \widetilde{N}_{x\theta}}{\partial x} + \frac{1}{R}\frac{\partial \widetilde{N}_\theta}{\partial \theta} + \frac{1}{R}\frac{\partial \widetilde{M}_{x\theta}}{\partial x} + \frac{1}{R^2}\frac{\partial \widetilde{M}_\theta}{\partial \theta}$$

$$b_3 = \frac{\partial^2 \overline{M}_x}{\partial x^2} + \frac{2}{R}\frac{\partial^2 \overline{M}_{x\theta}}{\partial x \partial \theta} + \frac{1}{R^2}\frac{\partial^2 \overline{M}_\theta}{\partial \theta^2} - \frac{\overline{N}_\theta}{R} + \frac{\partial^2 \widetilde{M}_x}{\partial x^2} + \frac{2}{R}\frac{\partial^2 \widetilde{M}_{x\theta}}{\partial x \partial \theta} + \frac{1}{R^2}\frac{\partial^2 \widetilde{M}_\theta}{\partial \theta^2} - \frac{\widetilde{N}_\theta}{R}$$

Appendix 2.

The normalized and discretized equations are shown as follows.

$$
\begin{aligned}
&(R^2/L)\cos(n\theta+\omega t)\sum_{l=2}^{N-1}A_{i,l}^{(2)}U_l+(-n^2A_{66}/A_{11}+f^{*2})L\cos(n\theta+\omega t)U_i\\
&+nR^2[(\frac{B_{12}}{R}+A_{12}+\frac{2A_{66}B_{66}}{R})/(LA_{11})]\cos(n\theta+\omega t)\sum_{l=2}^{N-1}A_{i,l}^{(1)}V_l-[B_{11}hR^2/(L^3A_{11})]\cos(n\theta+\omega t)\sum_{l=3}^{N-2}C_8W_l\\
&+\{[A_{12}R+n^2(B_{12}+2B_{66})]h/(LA_{11})\}\cos(n\theta+\omega t)\sum_{l=3}^{N-2}C_7W_l\\
&+\frac{hR^2}{LA_{11}}(-\omega)\sin(n\theta+\omega t)\sum_{k=1}^{N_m}\bar{e}_{31}k_cc(t)(Z_{k+1}-Z_k)h\sum_{l=3}^{N-2}C_7W_l\\
&+\frac{hR^2}{RA_{11}}(-\omega)n\cos(n\theta+\omega t)\sum_{k=1}^{N_m}\bar{e}_{36}k_cc(t)(Z_{k+1}-Z_k)hW_i=F_1
\end{aligned}
\tag{A2}
$$

$$
\begin{aligned}
&R^3[(A_{66}+\frac{3B_{66}}{R}+\frac{2D_{66}}{R^2}+N_a)/(L^2A_{11})]\sin(n\theta+\omega t)\sum_{l=2}^{N-1}A_{i,l}^{(2)}V_l\\
&-nR^2[(\frac{B_{12}}{R^2}+\frac{A_{12}}{R}+\frac{A_{66}}{R}+\frac{B_{66}}{R^2})/A_{11}]\sin(n\theta+\omega t)\sum_{l=2}^{N-1}A_{i,l}^{(1)}U_l\\
&+[-n^2R^3(\frac{2B_{22}}{R^3}+\frac{A_{22}}{R^2}+\frac{D_{22}}{R^4})/A_{11}+f^{*2}R)]\sin(n\theta+\omega t)V_i\\
&+[nhR^2(\frac{2B_{66}}{R}+\frac{B_{12}}{R}+\frac{2D_{66}}{R^2}+\frac{D_{12}}{R^2})/(L^2A_{11})]\sin(n\theta+\omega t)\sum_{l=3}^{N-2}C_4W_l\\
&+\{[-n(\frac{A_{22}}{R^2}+\frac{B_{22}}{R^3})-n^3(\frac{B_{22}}{R^3}+\frac{D_{22}}{R^4})]hR^2/A_{11}\}\sin(n\theta+\omega t)W_i\\
&+\frac{hR^2}{LA_{11}}(-\omega)\sin(n\theta+\omega t)[\sum_{k=1}^{N_m}\bar{e}_{36}k_cc(t)(Z_{k+1}-Z_k)h+\frac{1}{R}\sum_{k=1}^{N_m}\bar{e}_{36}k_cc(t)(\frac{Z_{k+1}^3-Z_k^3}{3})h^3]\sum_{l=3}^{N-2}C_7W_l\\
&(-hR^2\omega/A_{11})n\cos(n\theta+\omega t)[\frac{1}{R}\sum_{k=1}^{N_m}\bar{e}_{32}k_cc(t)(Z_{k+1}-Z_k)h+\frac{1}{R^2}\sum_{k=1}^{N_m}\bar{e}_{32}k_cc(t)(\frac{Z_{k+1}^3-Z_k^3}{3})h^3]W_i=F_2
\end{aligned}
\tag{A3}
$$

$$
\begin{aligned}
&\frac{B_{11}R^2}{L^2A_{11}}\cos(n\theta+\omega t)\sum_{l=3}^{N-1}A_{i,l}^{(3)}U_l-[(\frac{A_{12}}{R}+n^2\frac{B_{12}+2B_{66}}{R^2})R^2/A_{11}]\cos(n\theta+\omega t)\sum_{l=2}^{N-1}A_{i,l}^{(1)}U_l\\
&+[nR^3(\frac{2B_{66}}{R}+\frac{B_{12}}{R}+\frac{4D_{66}}{R^2}+\frac{D_{12}}{R^2})/(L^2A_{11})]\cos(n\theta+\omega t)\sum_{l=2}^{N-1}A_{i,l}^{(2)}V_l\\
&+\{[-n(\frac{A_{22}}{R^2}+\frac{B_{22}}{R^3})-n^3(\frac{B_{22}}{R^3}+\frac{D_{22}}{R^4})]R^3/A_{11}\}\cos(n\theta+\omega t)V_i-\frac{D_{11}hR^2}{L^4A_{11}}\cos(n\theta+\omega t)\sum_{l=3}^{N-2}C_1W_l\\
&+[(\frac{2B_{12}}{R}+n^2\frac{2D_{12}+4D_{66}}{R^2}+N_a)hR^2/(L^2A_{11})]\cos(n\theta+\omega t)\sum_{l=3}^{N-2}C_4W_l\\
&+\{[(-n^4\frac{D_{22}}{R^4}-n^2\frac{2B_{22}}{R^3}-\frac{A_{22}}{R^2})hR^2/A_{11}]+f^{*2}h\}\cos(n\theta+\omega t)W_i-hR^2\varpi/(L^2A_{11})W_i\\
&+\frac{hR^2}{L^2A_{11}}(-\omega)\sin(n\theta+\omega t)\\
&+\sum_{k=1}^{N_m}\bar{e}_{31}k_cc(t)(\frac{Z_{k+1}^3-Z_k^3}{3})h^3]\sum_{l=3}^{N-2}C_4W_l+\frac{2hR^2}{LA_{11}R}(-\omega)n\cos(n\theta+\omega t)\sum_{k=1}^{N_m}\bar{e}_{36}k_cc(t)(\frac{Z_{k+1}^3-Z_k^3}{3})h^3\sum_{l=3}^{N-2}C_7W_l\\
&+\frac{hR^2}{LA_{11}}(-\omega)\sin(n\theta+\omega t)[\frac{1}{R^2}\sum_{k=1}^{N_m}\bar{e}_{32}k_cc(t)(-n^2)(\frac{Z_{k+1}^3-Z_k^3}{3})h^3-\frac{1}{R}\sum_{k=1}^{N_m}\bar{e}_{32}k_cc(t)(Z_{k+1}-Z_k)h]W_i=F_3
\end{aligned}
\tag{A4}
$$

where

$$F_1=\int_{-\frac{h}{2}}^{\frac{h}{2}}(\overline{Q}_{11}\alpha_x+\overline{Q}_{12}\alpha_\theta+\overline{Q}_{16}\alpha_{x\theta})T_0dz$$

$$F_2=\int_{-\frac{h}{2}}^{\frac{h}{2}}(\overline{Q}_{16}\alpha_x+\overline{Q}_{26}\alpha_\theta+\overline{Q}_{66}\alpha_{x\theta})T_0dz$$

$$F_3 = \frac{-1}{R}\int_{-\frac{h}{2}}^{\frac{h}{2}} (\overline{Q}_{12}\alpha_x + \overline{Q}_{22}\alpha_\theta + \overline{Q}_{26}\alpha_{x\theta})T_0 dz$$

$$N_a = \frac{-A_{11}}{R^2}\int_{-\frac{h}{2}}^{\frac{h}{2}} (\overline{Q}_{11}\alpha_x + \overline{Q}_{12}\alpha_\theta + \overline{Q}_{16}\alpha_{x\theta})T_0 dz$$

$$C_8 = A_{i,l}^{(3)} - \frac{A_{i,2}^{(3)} \cdot AXK\ 1 + A_{i,N-1}^{(3)} \cdot AXKN}{AXN}$$

$$C_7 = A_{i,l}^{(1)} - \frac{A_{i,2}^{(1)} \cdot AXK\ 1 + A_{i,N-1}^{(1)} \cdot AXKN}{AXN}$$

$$C_4 = A_{i,l}^{(2)} - \frac{A_{i,2}^{(2)} \cdot AXK\ 1 + A_{i,N-1}^{(2)} \cdot AXKN}{AXN}$$

$$C_1 = A_{i,l}^{(4)} - \frac{A_{i,2}^{(4)} \cdot AXK\ 1 + A_{i,N-1}^{(4)} \cdot AXKN}{AXN}$$

$$AXN = A_{N,2}^{(2)} \cdot A_{1,N-1}^{(2)} - A_{1,2}^{(2)} \cdot A_{N,N-1}^{(2)}$$

$$AXK\ 1 = -(A_{1,l}^{(2)} \cdot A_{N,N-1}^{(2)} - A_{1,N-1}^{(2)} \cdot A_{N,l}^{(2)})$$

$$AXKN = -(A_{1,2}^{(2)} \cdot A_{N,l}^{(2)} - A_{1,l}^{(2)} \cdot A_{N,2}^{(2)})$$

Appendix 3.

The thermal stresses in discretized equation of the k^{th} layer are shown as follows.

$$\begin{aligned}\sigma_x =& [(\sum_{l=1}^{N} A_{i,l}^{(1)} U_l - \frac{h^2 Z}{L^2}\sum_{l=1}^{N} A_{i,l}^{(2)} W_l)\cos(n\theta+\omega t) - \alpha_x A_{11} T_0 LX_i / R^2]\overline{Q}_{11} \\ &+ \{[nRV_i + hW_i)/R - \frac{hZ}{R^2}(-n^2 W - n_i V_i)]\cos(n\theta+\omega t) - \alpha_\theta A_{11} T_0 LX_i / R^2\}\overline{Q}_{12} \\ &+ [\frac{R}{L}\sum_{l=1}^{N} A_{i,l}^{(1)} V_l - \frac{Ln}{R}U_i - \frac{2hZ}{R}(-\frac{nh}{L}\sum_{l=1}^{N} A_{i,l}^{(1)} W_l - \frac{R}{L}\sum_{l=1}^{N} A_{i,l}^{(1)} V_l)]\overline{Q}_{16}\sin(n\theta+\omega t) \\ &- \alpha_{x\theta}\frac{A_{11}}{R^2} T_0 LX_i \overline{Q}_{16} - \overline{e}_{31} k_c c(t)(-\omega)\sin(n\theta+\omega t) hW_i\end{aligned} \tag{A5}$$

$$\begin{aligned}\sigma_\theta =& [(\sum_{l=1}^{N} A_{i,l}^{(1)} U_l - \frac{h^2 Z}{L^2}\sum_{l=1}^{N} A_{i,l}^{(2)} W_l)\cos(n\theta+\omega t) - \alpha_x \frac{A_{11}}{R^2} T_0 LX_i]\overline{Q}_{12} \\ &+ \{[\frac{1}{R}(nRV_i + hW_i) - \frac{hZ}{R^2}(-n^2 W - n_i V_i)]\cos(n\theta+\omega t) - \alpha_\theta \frac{A_{11}}{R^2} T_0 LX_i\}\overline{Q}_{22} \\ &+ [\frac{R}{L}\sum_{l=1}^{N} A_{i,l}^{(1)} V_l - \frac{Ln}{R}U_i - \frac{2hZ}{R}(-\frac{nh}{L}\sum_{l=1}^{N} A_{i,l}^{(1)} W_l - \frac{R}{L}\sum_{l=1}^{N} A_{i,l}^{(1)} V_l)]\overline{Q}_{26}\sin(n\theta+\omega t) \\ &- \alpha_{x\theta}\frac{A_{11}}{R^2} T_0 LX_i \overline{Q}_{26} - \overline{e}_{32} k_c c(t)(-\omega)\sin(n\theta+\omega t) hW_i\end{aligned} \tag{A6}$$

$$\begin{aligned}\sigma_{x\theta} =& [(\sum_{l=1}^{N} A_{i,l}^{(1)} U_l - \frac{h^2 Z}{L^2}\sum_{l=1}^{N} A_{i,l}^{(2)} W_l)\cos(n\theta+\omega t) - \alpha_x \frac{A_{11}}{R^2} T_0 LX_i]\overline{Q}_{16} - \alpha_x \frac{A_{11}}{R^2} T_0 LX_i]\overline{Q}_{16} \\ &+ \{[\frac{1}{R}(nRV_i + hW_i) - \frac{hZ}{R^2}(-n^2 W - n_i V_i)]\cos(n\theta+\omega t) - \alpha_\theta \frac{A_{11}}{R^2} T_0 LX_i\}\overline{Q}_{26} \\ &+ [\frac{R}{L}\sum_{l=1}^{N} A_{i,l}^{(1)} V_l - \frac{Ln}{R}U_i - \frac{2hZ}{R}(-\frac{nh}{L}\sum_{l=1}^{N} A_{i,l}^{(1)} W_l - \frac{R}{L}\sum_{l=1}^{N} A_{i,l}^{(1)} V_l)]\overline{Q}_{66}\sin(n\theta+\omega t) \\ &- \alpha_{x\theta}\frac{A_{11}}{R^2} T_0 LX_i \overline{Q}_{66} - \overline{e}_{36} k_c c(t)(-\omega)\sin(n\theta+\omega t) hW_i\end{aligned} \tag{A7}$$